Available online at www.sciencedirect.com
SCIENCE DIRECT
Journal of Photochemistry and Photobiology A: Chemistry 181 (2006) 203–214
Journal of Photochemistry and Photobiology A:Chemistry
www.elsevier.com/locate/jphotochem

Photocatalytic activity and photo-induced superhydrophilicity of sol–gel derived TiO_2 films

M. Langlet [a,*], S. Permpoon [a,b], D. Riassetto [a], G. Berthomé [b], E. Pernot [a], J.C. Joud [b]

[a] *LMGP/ENSPG-INPG, BP 46, Domaine Universitaire, 38402 Saint Martin d'Hères, France*
[b] *LTPCM/ENSEEG-INPG, BP 75, Domaine Universitaire, 38402 Saint Martin d'Hères, France*

Received 9 November 2005; received in revised form 25 November 2005; accepted 27 November 2005
Available online 18 January 2006

Abstract

TiO_2 thin films have been deposited using various sol–gel routes. X-ray diffraction, ellipsometry, atomic force microscopy, and scanning electron microscopy characterizations show that the film morphology is strongly influenced by the sol nature and post-deposition heat-treatment temperature. Photo-induced properties of the films have been studied in relation to their morphology. In aqueous medium, photocatalytic properties are governed by a migration of photo-generated charge carriers, which occurs through the whole film thickness and closely depends on the film morphology, in particular the crystallization and densification degrees, as well as the primary and secondary particle sizes. Correlations between photocatalytic activity and photo-induced superhydrophilicity show that both properties are influenced by same mechanisms. Photo-wettability mechanisms are less critically influenced by morphologic properties because they only involve a very thin active surface layer.

Keywords: Sol–gel thin films; Titanium oxide; Photocatalysis; Photo-induced superhydrophilicity

1. Introduction

Since Fujishima and Honda have established that, under UV exposition, a TiO_2 electrode can decompose water to hydrogen and oxygen [1], photo-induced properties of titania, preferentially in its anatase polymorphic form, have been the object of a huge interest for many kinds of applications (see a very recent and complete review on the properties and applications of photoactive titanium oxide in [2]). For instance, photocatalytic properties of suspended titania powders have extensively been studied for environmental applications such as water decontamination and purification [3]. Photocatalytic reactions proceed under UV-irradiation, with photon energy equal to or greater than titania band gap energy (for anatase: $h\nu > 3.2$ eV, i.e. $\lambda < 380$ nm), which yields free photoelectrons (e^-) and holes (p^+). These photo-generated charge carriers are then able to interact through multi-step redox mechanisms with organic matter present at a TiO_2 particle surface. Many papers have been devoted to the effects of grain morphology on the activity of TiO_2 powdered photocatalysts [4–8]. Small crystallites beneficially impact photocatalytic properties by increasing the number of active surface sites in contact with matter to be photocatalytically decomposed and by minimizing the risks of charge carrier recombination within the particle volume. However, small particles also favor an enhanced e^-/p^+ surface recombination rate, which offsets the benefits of high surface area. Volume and surface recombination are known to be important parasitic mechanisms that can totally cancel the photoactivity. Accordingly, the devoted literature shows a complex influence of grain size on the properties of powdered photocatalysts, and results are rather conflicting. Some authors mentioned an ideal crystal size smaller than 10 nm [4,5], while other authors claimed that best photocatalytic activity was reached for a crystal size of 15–25 nm [6,7]. In any cases, reported particle sizes were claimed to be ideal compromises for minimization of surface and volume recombination rates. Besides, during the preparation of titania powders, primary single-crystal particles can agglomerate leading to secondary polycrystalline particles of various sizes, which depend on the synthesis routes. The size of secondary particles can also greatly influence photocatalytic properties. Accordingly, several authors mentioned the complex and interactive influence of primary and secondary par-

* Corresponding author. Tel.: +33 4 76 82 63 25; fax: +33 4 76 82 63 94.
E-mail address: Michel.Langlet@inpg.fr (M. Langlet).

1010-6030/$ – see front matter © 2005 Elsevier B.V. All rights reserved.
doi:10.1016/j.jphotochem.2005.11.026

ticle sizes on the photocatalytic properties of TiO_2 powders [5,7,8].

When titania is immobilized on a rigid support in the form of a thin film, new photocatalytic applications can be envisaged that have been largely investigated over the past decade, including supported photocatalysts for water purification [9], antibacterial surfaces [10], or photoactive surfaces for deodorizing or purifying indoor atmospheres [11]. Interest for TiO_2 films has broadened again after the recent finding that titania surfaces exhibit a photo-induced superhydrophilicity, i.e. a water contact angle of zero under UV exposure [12]. This property arises from photo-generated holes that create oxygen vacancies at the titania surface. Oxygen vacancies are then able to promote the molecular or dissociative adsorption of water, leading to superhydrophilicity. This property has, for instance, largely been studied for antifogging surface applications [13]. Among the different applications of photoactive TiO_2 thin films, one of the most studied concerns self-cleaning surfaces [14,15], which rely both on photocatalysis and photo-hydrophilicity mechanisms. Photocatalytic properties yield the partial or total decomposition of pollutant organic matter present at the surface, while photo-induced superhydrophilicity allows elimination of remaining organic contamination through a simple water rinsing operation without the need of detergent. Over the last decade, many self-cleaning products have been commercialized in Japan, USA, Europe, and other countries in the world.

In contrast to powdered photocatalysts, influence of the grain morphology on the photoactivity of TiO_2 films has not been extensively studied. In a recent paper, Mills et al. have indicated that the photocatalytic activity of very thick films (around 4.5 μm in thickness) readily increases with porosity [16]. In this work, photodecomposition experiments were performed in solid phase, using stearic acid as a model molecule, which involved gaseous oxygen as a co-reactant. In different photocatalysis experimental conditions, i.e. photodecomposition experiments performed in aqueous medium that involve water as a co-reactant, we have previously shown that, provided that the pore size is small enough for preventing liquid pollutant penetration within the film, the photocatalytic activity of TiO_2 films is governed by a migration of photo-generated charge carriers from the deeper layers toward the film surface, and this mechanism is strongly influenced by elaboration conditions of the films [17,18]. Powdered catalyst applications generally involve suspended titania particles in direct contact with the matter to be photocatalytically decomposed, which means that risks of charge carrier recombination are restrained to the volume and surface of primary or secondary particles. In the case of a polycrystalline film with a given thickness, charge carrier migration toward the surface involves multi-grain interfacial transfers. It implies that, compared to a powdered photocatalyst, the probability of e^-/p^+ recombination should be much greater owing to multi-recombination within grain volumes and at grain interfaces. Consequently, at least two essential additional parameters can influence the photoactivity of TiO_2 films in aqueous medium: the film thickness (the recombination probability of charge carriers should increase with a thickness increase owing to a longer migration pathway) and the film porosity (a greater pore size should impinge the inter-granular transfer and favor a greater recombination at the grain surface during migration). It can thus be inferred that the photoactivity dependence on the grain size will show more complex trends in the case of a film, and the optimal grain size can be very different from that for a powdered photocatalyst. Furthermore, the grain size can also strongly influence the film roughness, which can in turn modify surface properties involved in the photoactivity, i.e. adsorption of a pollutant to be photocatalytically decomposed or water adsorption that governs the photo-hydrophilicity mechanism.

In this work, sol–gel TiO_2 thin films were deposited from different precursor sols and heat-treated at various temperatures. Hereafter, we present their photo-induced catalytic and superhydrophilic properties. These properties are discussed with respect to the film thickness and morphology.

2. Experimental

2.1. Sol and film preparation

TiO_2 films were deposited from various sols. A mother sol (MS) was prepared from tetraisopropyl orthotitanate (TIPT from Fluka) diluted in absolute ethanol with a TIPT concentration $C_{TIPT} = 0.4$ mol/l, a pH of 1.27, and a water to TIPT molar ratio $r_w = 0.8$. Crystalline suspensions (CS) of TiO_2 nanoparticles in ethanol were prepared from this mother solution following a multi-step procedure, including dilution of the mother solution in various water amounts and subsequent autoclaving. The whole preparation procedure has been detailed in previous papers [17,18]. In these papers, we showed that the autoclaved suspensions were composed of well-crystallized and aggregated anatase particles and the primary and secondary particle sizes decreased with increasing the r_w ratio. We also showed that the crystallite size slightly increased with increasing autoclaving temperature. In the present work, the r_w ratio has been adjusted between 10 and 90 and autoclaving temperature has been fixed at 130 or 200 °C.

Films were deposited from MS and CS sols by spin-coating (20 μl; 6000 rpm) on Si(1 0 0) wafers of identical size (3.3 cm × 3.3 cm). The different sols yielded a similar surface coverage. 90% of the substrate surface was coated with a thickness uniformity of about 1%. The other 10% corresponded to unavoidable edge and corner effects, where the thickness was greater than in the homogenously coated area. In this study, thickness values correspond to those measured in the homogeneous area. All the films presented hereafter exhibited high and similar optical quality. The whole film preparation procedure has been detailed in [18]. After liquid film deposition, the MS sol reacted through the well-known hydrolysis/polycondensation sol–gel routes leading to an amorphous xerogel film, while the CS sols yielded polycrystalline films after solvent evaporation. Hereafter, the film nomenclature corresponds to the sol formulation, i.e. MS films or CS/r_w/T films (for instance, CS/90/130 for a film deposited from a crystalline suspension autoclaved at 130 °C with r_w ratio of 90). After deposition, the films were heat-treated for 2 h at temperatures up to 700 °C. Higher heat-treatment temperatures yielded an anatase/rutile phase

transformation. Rutile is known to be less photocatalytically active than anatase. Thus, in this work we only focused on anatase films heat-treated at 700 °C or less. The film thickness was adjusted using a multi-layer deposition procedure. Ellipsometric measurements showed that the film thickness, measured after heat-treatment, linearly increased with the number of single-coatings. Film thicknesses up to 500 nm were studied. Very thin films of 40 nm thickness or less were also deposited, using a single-deposition run, after further dilution in ethanol of precursor sols.

2.2. Film characterization

X-ray diffraction (XRD) characterizations were performed using a Siemens D5000 diffractometer with Cu $K\alpha_1$ radiation ($\lambda = 1.54056$ Å). The diffracted intensity was recorded in a [22–60°] 2θ range with a step of 0.02° and an integration time of 22 s. The average crystallite size of MS and CS films was estimated, using Scherrer's formula, from the full width at half maximum (FWHM) of the (1 0 1) reflection of anatase corrected from the diffractometer resolution. Film thickness and refractive index were measured using a Sentech ellipsometer at 632 nm wavelength. The volume porosity (P in vol%) was estimated from the film refractive index (n) using the Lorentz–Lorenz relationship [19]

$$1 - \frac{P}{100} = \frac{n^2 - 1}{N^2 - 1} \times \frac{N^2 + 2}{n^2 + 2}$$

where N corresponds to the bulk material refractive index ($N \approx 2.50$ for anatase [20]).

Film surface morphologies were studied by scanning electron microscopy (SEM), using a Philips XL 30 apparatus, and atomic force microscopy (AFM), using a Digital Instrument Nanoscope Multi-mode apparatus. AFM data, collected by Tapping Mode imaging using a silicon tip with a radius of curvature less than 5 nm, were computed from spectral analysis. Surface chemical analysis was performed by X-ray photoelectron spectroscopy (XPS) using a XR3E2 apparatus from Vacuum Generator employing an Mg Kα source (1253.6 eV). Before collecting data, the samples were put in equilibrium for 24 h in an ultra high vacuum chamber (10^{-10} mbar). Photoelectrons were collected by a hemispherical analyzer at 30° take-off angle.

The photocatalytic activity was measured at room temperature. Titania films were settled in a Pyrex photoreactor opened to air containing malic (2-hydroxybutanedioic) acid aqueous solution (30 ml; 3.7×10^{-4} M; natural neutral pH). Constant agitation of the solution was insured using a magnetic stirrer. Before UV-irradiation, the solution was first stirred in the dark for 60 min to reach equilibrated adsorption of malic acid at the film surface. The film was then exposed for 3 h to UV-irradiation provided by a Philips HPK 125 UV-lamp (40 mW/cm^2 at the film surface) using a Corning 0.52 filter ($\lambda > 340$ nm). To avoid heating of the solution during irradiation, light was passed through a circulating-water cuvette located between the photoreactor and the lamp. Small solution aliquots were periodically withdrawn in order to measure the concentration variations of malic acid as a function of time. Malic acid analysis was performed by liquid chromatography (HPLC) using a Waters 600 chromatograph, equipped with a SARASEP CAR-H column (eluent: H_2SO_4, 5×10^{-3} M; flow rate: 0.7 ml/min; detection at $\lambda = 210$ nm). The photocatalytic activity was determined from the rate of disappearance of malic acid. This acid has been chosen as a model molecule of carboxylic acids, which are the best representatives for the main constituents of intermediate products in oxidative degradation processes [21].

Wettability properties were systematically measured within the first 24 h following film deposition. Films aged for 1 week were also studied in some cases. The natural hydrophilicity of TiO_2 films was quantified from measurements of the water contact angle in the absence of UV light. Experiments were performed at 20 °C in an environmental chamber using a KRUSS G 10 goniometer connected with a video camera. Several water droplets of 0.5 μl volume were spread on the samples and water contact angles were measured at different points of the thin film surface for statistical purpose. The photo-induced film hydrophilicity was evaluated, using a same statistical procedure, from the in-time variations of the water contact angle under UV light irradiation. For these experiments, we used a 100 W black light mercury lamp (B-100AP, Ultraviolet Product Co. Ltd.) principally emitting at a 365 nm wavelength. Any higher energy emission lines were suppressed using a devoted filter. Except when otherwise mentioned in the text, the distance between the lamp and the film was fixed at 5 cm, which provided a light intensity of 21 mW/cm^2 at the film surface. Photo-hydrophilic properties have been characterized by the so-called photo-wettability duration, which depicts the UV illumination duration necessary for inducing a superhydrophilic surface with a water contact angle of zero.

3. Results and discussion

3.1. Morphology features

The morphology of MS and CS films varied only weakly with respect to thickness. It means that the multi-layer deposition procedure did not greatly affect morphological features, which were essentially influenced by the sol nature and post-deposition heat-treatment temperature. In the present section, we focus therefore on these parameters. It is worthwhile mentioning that all films presented hereafter exhibited similarly high optical qualities. Spectroscopic measurements (not illustrated here) showed that optical transmission losses induced by absorption or diffusion were below 1% in the visible spectral range. The film optical quality is a parameter of importance because absorption and diffusion mechanisms can significantly alter the optical pathway of UV light within film thickness, which can in turn modify the charge carrier photogeneration and related photo-induced properties. Owing to the similar optical quality of films studied hereafter, it is inferred that differences in their photo-induced properties did not relate to absorption or diffusion variations. Reflection at the film–air interface, which increases with the refractive index value, can also influence the fraction of UV light that penetrates the film and modify the charge carrier photogeneration. This aspect will be assessed in next section.

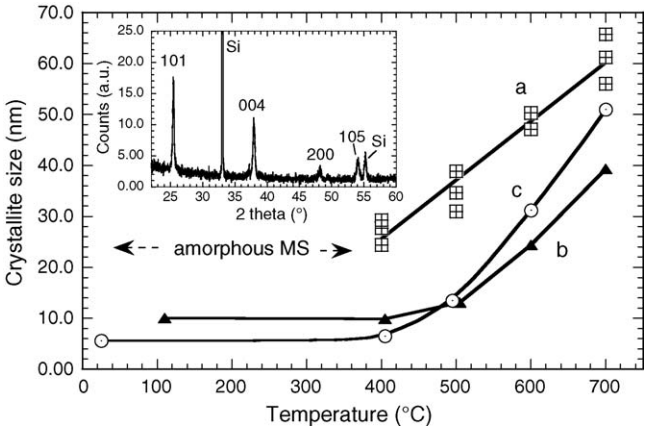

Fig. 1. Variations of crystallite size with annealing temperature for: (a) MS, (b) CS/10/200 and (c) CS/90/130 films. Inset shows the typical XRD pattern of a MS film heat-treated at 700 °C with indexed anatase reflections.

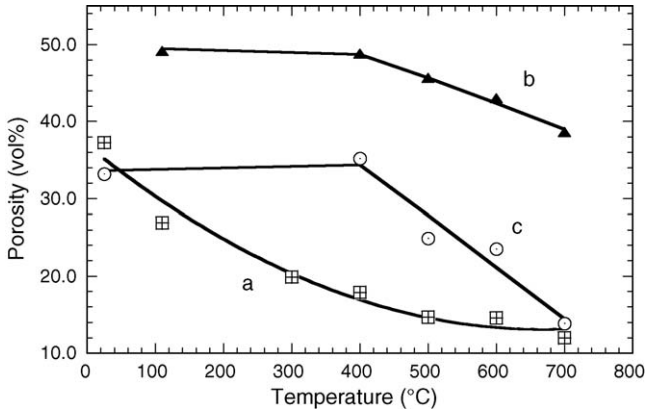

Fig. 2. Volume porosity, as deduced from the refractive index value, for: (a) MS, (b) CS/10/200 and (c) CS/90/130 films heat-treated at various temperatures.

XRD patterns of MS films heat-treated up to 350 °C did not exhibit any reflection showing the formation of amorphous films. For MS films heat-treated at 400 °C or more, and for all CS films, XRD patterns exhibited well-resolved reflections of a pure anatase phase (see, for instance, the XRD pattern of a MS film heat-treated at 700 °C in inset of Fig. 1). Previous XPS studies showed that the Ti^{3+}/Ti^{4+} ratio in crystalline MS and CS films was about 3 at%, which indicated a similarly high oxidation degree of these films [22]. The net area of the (1 0 1) anatase reflection was observed to increase by about 20–30% with increasing heat-treatment temperature up to 700 °C (not illustrated here), depicting a certain increase of the crystallization degree. Fig. 1 shows the crystallite size determined from the (1 0 1) anatase reflection for MS, CS/10/200 and CS/90/130 films heat-treated at various temperatures. Size values derived from XRD measurements were confirmed by punctual transmission electron microscope (TEM) observations (not illustrated here). Non-annealed CS/90/130 and CS/10/200 films exhibit an average crystalline size of 6 and 10 nm, respectively. This observation is in agreement with previous TEM studies showing that the size of crystallites formed during sol autoclaving slightly increased with decreasing (increasing) the r_w ratio (autoclaving temperature) [17,18]. Fig. 1b and c shows that the crystallite size does not vary appreciably when heating CS films up to 400 °C. Heat-treatments at higher temperature yield a marked crystal growth. Crystal sizes of around 40 and 50 nm are measured after heat-treatment at 700 °C for CS/10/200 and CS/90/130 films, respectively. We have previously shown that crystal growth in CS films proceeds through a thermally activated mechanism governed by atom mobility at grain boundaries [18]. Since as-deposited CS/10/200 films have a greater crystallite size, i.e. a smaller apparent surface energy, the thermal crystal growth is less marked than for CS/90/130 films with smaller initial crystallite sizes [23]. The crystallite size of MS films heat-treated at 400 °C or more also increases with increasing temperature. It has been reported that, for TiO_2 films derived from a traditional polymeric sol that leads to the room temperature deposition of an amorphous xerogel films, i.e. films similar to our MS films, crystal growth proceeds through a thermally activated Avrami mechanism [24]. The Avrami model depicts a nucleation/growth process in the amorphous phase and has generally been used to describe thermally assisted crystallization in gels derived from a sol–gel route [25]. Since in the amorphous state atom mobility is fast, crystals rapidly grow and MS films heated at 400 °C are constituted of much larger crystal (around 25 nm in size) than CS films heated at a same temperature. When crystallization proceeds, atom mobility diminishes and the difference between MS and CS film decreases with increasing temperature as shown in Fig. 1. The average crystallite size of MS films heated at 700 °C was approximately 60 nm.

Ellipsometric measurements showed that the film refractive index closely depended on the sol nature and post-deposition heat-treatment temperature. For films studied here, no anatase/rutile phase transformation occurred, which could induce a refractive index increase. It is therefore concluded that index variations essentially depict densification features. Fig. 2 shows that a wide range of porosities, between 12 and 50 vol%, can be covered depending on the experimental conditions. For amorphous MS films heat-treated up to 350 °C, the porosity decreases markedly with increasing temperature. Since these films are deposited from titanium alkoxide and alkoxy groups generally require a heat-treatment between 300 and 350 °C to be fully decomposed [26], it is not excluded that the porosity of amorphous films be slightly underestimated, i.e. residual alkoxy groups might partially fill pores of the film leading to an increase of the refractive index value. For MS films crystallized at 400 °C or more, the porosity decrease with increasing temperature is less pronounced. This trend illustrates that in the amorphous state, densification proceeds through a viscous flow mechanism while atomic diffusion is involved in the case of crystalline materials, and that the former mechanism is much faster than the latter [25]. Generally speaking, Fig. 2 shows that porosity of crystalline films, i.e. MS films heated at 400 °C or more and all CS films, follows trends similar to those of crystallite size illustrated in Fig. 1. On the one hand, crystallite sizes and densification degrees of MS films continuously increase with increasing temperature. On the other hand, no significant crystallite size and porosity variations are observed for CS films heat-treated up to 400 °C, while densification and crys-

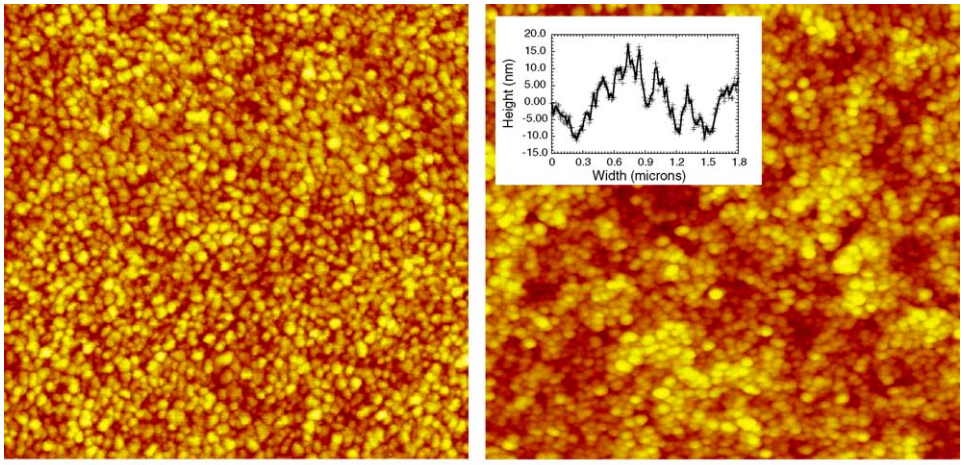

Fig. 3. AFM images (1 μm × 1 μm areas) of: (a) a MS film and (b) a CS film heat-treated at 500 °C. Inset shows the local profile of the CS film thickness.

tal growth markedly proceed at higher temperatures. Besides, the porosity difference between MS and CS/90/130 films decreases with increasing temperature similarly to what is observed for crystallite size. These similarities express that, for each kind of films, common mechanisms govern crystal growth and densification, i.e. the thermally activated densification is associated with a nucleation/growth process for MS films and with atomic diffusion at grain boundaries for CS films. However, an essential discrepancy between Figs. 1 and 2 has to be underlined. While for CS/10/200 and CS/90/130 films crystallite size variations illustrated in Fig. 1 are rather similar, Fig. 2 shows that porosity of the former films is much greater than that of the latter and it decreases less markedly with increasing temperature. These features can be explained in the light of following microscopic observations.

Fig. 3 shows AFM pictures of MS and CS/90/130 films heat-treated at 500 °C. Both samples are characterized by a finely divided granular morphology with small inter-granular pores. The MS film surface (Fig. 3a) is very homogeneous, while the CS film exhibits smooth relief variations, which can be appreciated in Fig. 3b by marked color contrasts that do not appear in Fig. 3a. The typical local profile of such a relief is illustrated in the inset of Fig. 3b. The level differences between height maxima and minima statistically ranged between 15 and 30 nm. We previously showed that, in CS sols, anatase crystallites are aggregated in the form of polycrystalline particles [17]. During the post-deposition solvent evaporation stage, these aggregates pack more or less efficiently and can agglomerate, which presumably causes profile variations observed in Fig. 3b. For both films, spectral analysis indicated an average apparent grain size of 30–35 nm. It is worthwhile mentioning that, in the case of very small grains, sizes determined by AFM correspond to a convolution of tip and grain dimensions and do not necessarily account for the actual grain size. In other words, since the tip cannot probe the whole depth of very small pores, the apparent grain size determined by AFM also accounts for the inter-granular porosity. Thus, it is inferred that the value determined by AFM more reasonably corresponds to the "top-to-top" inter-granular distance. For the MS film illustrated in Fig. 3a, this inter-granular distance closely agrees with the crystallite size deduced from XRD measurements. It is thus concluded that grains observed in Fig. 3a are single-crystal particles that are separated by extremely small pores with a typical size of a few tens of nanometers. In contrast, the inter-granular distance measured by AFM for the CS film is about twice greater than the crystallite size deduced from XRD, which suggests a greater pore size of 10 nm or more. These pore sizes can in turn be related to differences in the volume porosity of MS and CS/90/130 films, as shown in Fig. 2. A RMS roughness smaller than 1 nm was measured for the MS film illustrated in Fig. 3a. Roughness is presumably caused by crystallites at the film surface. For the CS film (Fig. 3b), the RMS roughness was about five times greater. This greater value can arise from a convolution of the nanoroughness induced by crystalline particles and a larger roughness caused by aggregates.

All CS films studied here exhibited a similar granular morphology with aggregated crystallites. However, aggregate sizes and related inter-aggregate porosities closely depended on the CS sol formulation. This is illustrated in Fig. 4 for CS/10/200 and CS/90/130 films. Fig. 4c confirms AFM observations showing that CS/90/130 films are rather smooth. Similar surface morphologies were observed for all CS films issued from sols with r_w ratio of 30 or more. In contrast, the CS/10/200 film exhibits a more inhomogeneous surface with much larger aggregates and inter-aggregate pores (Fig. 4a and b). These inter-aggregate pores have a size of about 100 nm. We previously showed that CS sols autoclaved with a ratio below 30 were constituted of larger aggregates than CS sols with greater r_w [17]. During the post-deposition solvent evaporation step, larger aggregates presumably pack less efficiently, which causes the formation of large inter-aggregate pores. These large pores can in turn explain the greater volume porosity depicted by ellipsometry for CS/10/200 films (Fig. 2b). Another interesting feature is illustrated in Fig. 4a and b, which show the surface morphology of CS/10/200 films before and after heat-treatment at 700 °C, respectively. Both films exhibit large aggregates and inter-aggregate pores. Nevertheless, the inter-aggregate

porosity seems to be more pronounced after heat-treatment than before. It suggests that the thermally activated densification of CS films does not proceed through an inter-aggregate sintering mechanism, which would yield a reduction of the inter-aggregate porosity, but more presumably occurs within aggregates, which can in turn favor a closer contact between single-crystals and their subsequent growth through atom diffusion at grain boundaries. The intra-aggregate densification can also promote a reduction of the aggregate size and thus an increase of the inter-aggregate pore size. The competition between densification within aggregates and enlargement of inter-aggregate pores can in turn explain why the volume porosity decreases less markedly with increasing temperature for CS/10/200 films (Fig. 2b) than for CS films deposited from sols with greater r_w ratio (Fig. 2c). Fig. 5 shows roughness variations with temperature determined by AFM for MS and CS films. On the one hand, no significant variation can be evidenced for MS films that exhibit a very weak roughness at any temperatures. On the other hand, CS/10/200 and CS/90/130 films exhibit a rather similar roughness despite their very different surface morphologies illustrated in Fig. 4. The RMS roughness of as-deposited CS films is about 10 times greater than that measured for MS films, and it is observed to decrease with increasing temperature. After heat-treatment at 700 °C, the roughness is approximately twice weaker than before heat-treatment. This roughness decrease presumably ensues from the intra-aggregate densification mechanism and related crystal growth.

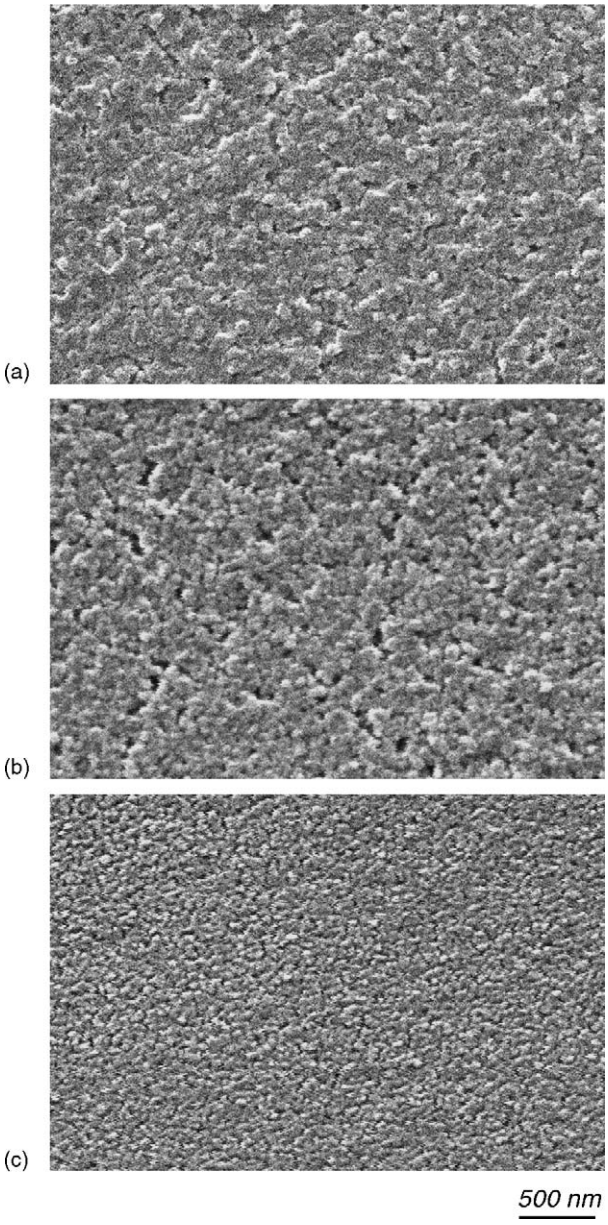

Fig. 4. SEM surface images of a CS/10/200 film (a) non-annealed or (b) annealed at 700 °C, and (c) a CS/90/130 film annealed at 700 °C. Magnification was ×40, 000.

3.2. Photocatalytic properties

Blank UV-irradiations performed for 3 h without titania films did not allow to detect any variation of the malic acid concentration, which indicated that no photolysis occurred over the whole duration of the photocatalytic experiments. After exposing the films in the dark for 60 min, the solution concentration was observed to decrease by 1–2 mol%, indicating malic acid adsorption at the film surface. The sensitivity of our measurements did not allow any correlation between the adsorption yield and experimental conditions (sol formulation, film thickness, heat-treatment temperature). In the presence of the films, the malic acid photodecomposition systematically followed a first order kinetics over a period of 120 min or more, i.e. the term $\ln(C_0/C)$ (where C_0 and C account for the malic acid concentration before and after exposition, respectively) linearly increased with UV exposition time (see inset of Fig. 6). Photodecomposition was observed to slow down for longer exposure durations. No film degradation could be observed after photocatalysis experiments, which might explain such a feature. It is therefore likely that a decomposition threshold exists, above which the malic acid decomposition is slower. In this work, the photocatalytic activity has been defined as the mole percentage of malic acid decomposed after 120 min UV exposure. Since for a true heterogeneous catalytic regime, the reaction rate linearly increases with the mass of catalyst [21], photocatalytic activities presented here-

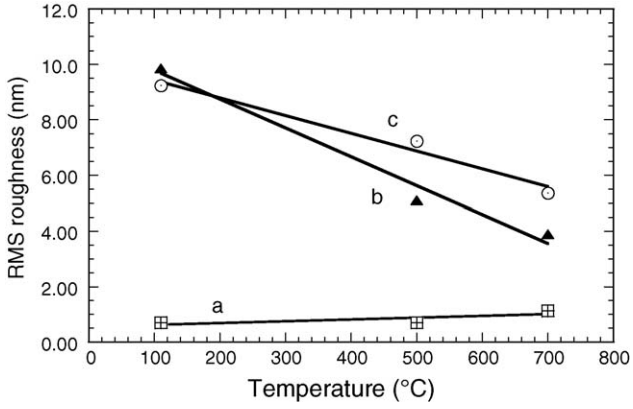

Fig. 5. RMS roughness determined by AFM on 40 μm × 40 μm areas for: (a) MS, (b) CS/10/200 and (c) CS/90/130 films heat-treated at various temperatures.

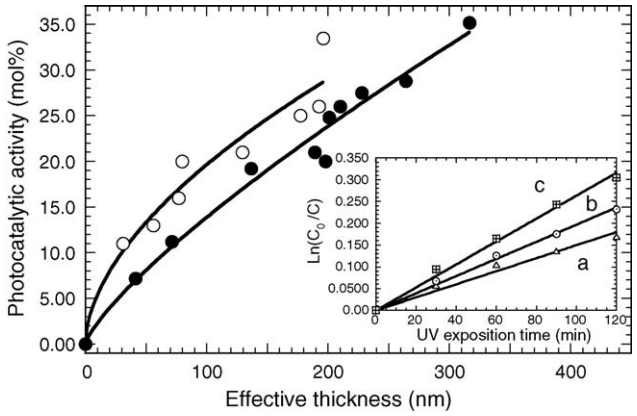

Fig. 6. Thickness dependence of the photocatalytic activity, expressed as the molar percentage of malic acid decomposed after 2 h UV exposure, for as-deposited CS/30/200 (●) and CS/90/130 films (○). Inset illustrates the photodecomposition kinetics for CS/90/130 films of: (a) 110 nm, (b) 185 nm and (c) 275 nm thickness.

after have been studied with respect to the so-called effective film thickness, i.e. the term $t \times (100 - P)$, where t and P are the films thickness and percentage of volume porosity for a given film, respectively. For a fixed substrate size, this effective thickness accounts for the actual amount of solid photocatalyst deposited on the substrate [18].

We previously indicated that the photocatalytic activity of TiO_2 films in aqueous medium was predominantly governed by a migration of photo-generated charge carriers within the whole film thickness, i.e. from the deeper layers toward the film surface [17,18]. This is illustrated in Fig. 6, which shows variations of the photocatalytic activity as a function of effective thickness for as-deposited CS/30/200 and CS/90/130 films. Let us note that these films only differed in their porosity, which was determined to be 40 vol% for the former and 30 vol% for the latter. Other morphologic properties were comparable for both films, including crystal size and aggregate size, and similar to those depicted in Fig. 3b. Fig. 6 shows that the photocatalytic activity gradually increases with film thickness, meaning that the inner part of films participates to malic acid photodecomposition, and for a same effective thickness (catalyst amount) the denser CS/90/130 films exhibits greater activity. This feature illustrates that a too high porosity impinges the inter-granular transfer, thus limiting the flux of charge carriers that reach the film surface and reducing the photocatalytic activity of the film. However, Fig. 6 also indicates that the activity increases more slowly than the film thickness. This is particularly marked for the denser film. For this film, the charge carrier recombination probability is greater owing to a more important flux of photo-generated electron and holes, and this probability increases with film thickness, i.e. with the migration pathway toward the surface, which leads to a progressive reduction of the photocatalytic yield. It is not excluded that participation of deeper layers of the film to the photocatalytic reaction can also arise from an impregnation of the liquid within pores, which would increase the number of active site. However, AFM studies suggested that, for films illustrated in Fig. 6, the inter-granular pore size was very small (around 10 nm), which should prevent significant liquid impregnation. Furthermore, the reactant impregnation should be favored by a greater porosity and, for a same effective thickness, the photoactivity of more porous films should be stronger than that of dense films. This assumption is denied by variations illustrated in Fig. 6. Finally, it has also to be recalled that more porous films exhibit a smaller refractive index. Thus, weaker reflection losses are induced at the surface of more porous films, which should in turn promote a better penetration of UV light within the film and a more efficient photogeneration of charge carriers. Refractive index values of around 1.7 and 1.8 were measured at 632 nm for CS/30/200 and CS/90/130 films, respectively. The former film should thus suffer weaker reflection losses. However, this film exhibits smaller photocatalytic activity than the latter. It suggests therefore that reflection losses do not influence greatly photocatalytic properties. All these features indicate that photocatalytic properties are predominantly influenced by a charge carrier migration mechanism.

This migration is in turn strongly influenced by morphologic characteristics and this influence appears to be rather complex. This is illustrated in Fig. 7, which shows the photocatalytic activity of MS, CS/10/200 and CS/90/130 films heat-treated at various temperatures. Since the photoactivity varies with the amount of photocatalyst, we have plotted the specific activity of the film, i.e. the photocatalytic activity normalized to the previously defined effective thickness. This specific activity accounts for the intrinsic activity of each active site [8], which in turn relies on surface or volume recombination probability and efficiency of the inter-granular charge carrier transfer. Moreover, since the photoactivity does not vary linearly with film thickness, we have compared films with rather similar effective thicknesses of 150–200 nm. Amorphous MS films heat-treated up to 350 °C did not show any activity. It is because, in amorphous phase, structural defects and impurities act as recombination centers promoting fast recombination of photo-generated charge carriers. Fig. 7a shows that the activity of crystalline MS films strongly increases when increasing the temperature up to 500–600 °C, which primarily ensues from an increase of the crystallization degree, i.e. a decrease in the fraction of recombination centers related to structural impurities. As shown in first section, the thermally activated film crystallization is accom-

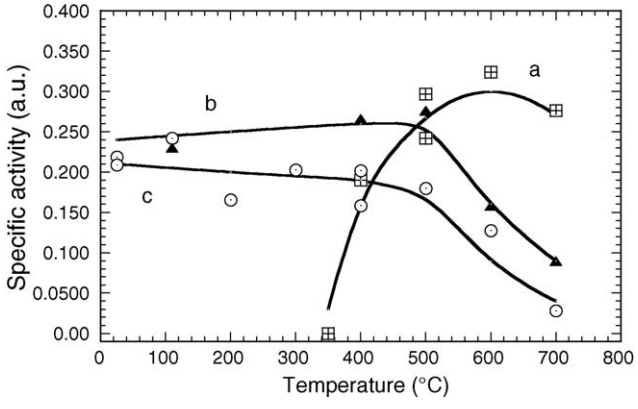

Fig. 7. Specific photocatalytic activity vs. annealing temperature for: (a) MS, (b) CS/10/200 and (c) CS/90/130 films.

panied with a reduction of the porosity. Denser films favor a more efficient inter-granular migration of the charge carriers, which also participates in the enhanced activity, despite stronger reflection losses induced by a greater refractive index that can reduce UV penetration in the films. However, further temperature increase does not yield any increase of the activity, which seems even to diminish after heating at 700 °C. This behavior suggests an influence of the crystallite size, which would affect the recombination of charge carriers during their migration toward the film surface. For crystalline MS films heat-treated at lower temperatures, smaller crystallites should favor the predominance of recombination at the grain surface owing to a greater surface area. Furthermore, for these films the residence time of charge carriers at the grain surface should be longer owing to a greater inter-granular porosity that impinges interfacial transfer of charge carriers. This should again enhance the surface recombination probability. When increasing temperature, surface area, and porosity decreases should favor a weaker surface recombination probability and better interfacial transfer, yielding an activity enhancement. However, at too high a temperature, larger crystallites should favor volume recombination within grain, thus offsetting the benefits of smaller surface area. It seems therefore that data illustrated in Fig. 7a illustrate a competition between surface and volume recombination, which would be conjointly minimized by optimizing the grain size after heat-treatment at 500–600 °C. According to Fig. 1a, this temperature would correspond to an optimum crystallite size comprised between 30 and 50 nm. This optimum size is significantly greater than that usually reported for unsupported powdered photocatalysts [4–7]. It is because in thin films, charge carrier migration toward the surface proceeds through multiple inter-granular transfers, which strongly modifies the photoactivity dependence on grain size compared to suspended powders.

Fig. 7b and c shows that the photoactivity of as-deposited CS films is 25–30% weaker than that of best MS films. Despite their rather good crystallization degree that promotes an efficient charge carrier generation, as-deposited CS films are more porous than crystallized MS films (Fig. 2), which yields a less efficient inter-granular transfer. The photoactivity of CS films weakly varies when increasing temperature up to 500 °C, which can be related to very weak variations of crystallite size and porosity illustrated in Figs. 1 and 2 for these films. The photoactivity of CS films significantly decreases when increasing temperature from 500 to 700 °C, despite a marked increase of their densification degree and crystallite size. For instance, the photoactivity of a CS/90/130 film annealed at 700 °C is about three times weaker than that measured for a MS film annealed at 600 °C, despite comparable crystallite size (50 nm) and volume porosity (14 vol%). These features suggest that, in contrast to MS films, the photoactivity is not directly governed by recombination mechanisms occurring at the primary particle surface or volume, but should more likely be influenced by secondary aggregated particles. Because thermal densification of CS films, which occurs above 400 °C, essentially takes place within aggregates, inter-granular transfer within aggregates is enhanced with increasing temperature. Denser aggregates can thus more or less behave like large single-crystals where volume recombination of charge carriers predominates. Volume recombination can in turn reduce the flux of charge carriers reaching the film surface in contact with matter to be decomposed. All CS films issued from sols with r_w ratio of 30 or more exhibited similar photoactivity variations with temperature, which could be related to their comparable morphology. In contrast, Fig. 7b and c shows that, at any temperatures, CS/10/200 films have a greater photoactivity than CS/90/130 films despite a much greater porosity. This observation might appear to be in contradiction with previous features showing that denser films are more active than porous ones. However, we have shown that CS/10/200 films exhibit a very particular morphology, with large pore sizes that were not observed for any other CS films deposited from sols with r_w ratio of 30 or more. It is therefore likely that, in the case of CS/10/200 films, liquid reactant is able to impregnate large pores and to partially penetrate deeper layers of the film. This would not only yield an enhanced contact surface between photocatalytic particles and matter to be decomposed, but would also imply a shorter migration pathway of charge carriers generated in the deepest layers of the film toward the contact surface, thus decreasing the recombination probability during migration. It is therefore believed that, contrary to other CS films where photoactivity predominantly depends on a charge carrier migration, the photoactivity of CS/10/200 films is governed not only by a migration mechanism, which explains that these films exhibit trends similar to other CS films with respect to temperature, but also by liquid impregnation, which favors an enhanced activity compared to CS/90/130 films. Besides, since CS/10/200 films are much more porous than CS/90/130 films, their refractive index is much weaker. For instance, values of around 1.55 and 1.8 were measured at 632 nm for the former and the latter, respectively, when heat-treated at 400 °C or less. Thus, it cannot be excluded that much weaker reflection losses induced at the surface of the former participate in a more efficient charge carrier photogeneration and then in a greater photocatalytic activity.

3.3. Photo-induced superhydrophilicity

As explained in introduction, the photo-induced superhydrophilicity of TiO_2 surfaces acts complementary to photocatalytic properties to promote a self-cleaning functionality. We previously showed that MS films heat-treated at 500 °C and as-deposited CS films exhibited similarly good photo-hydrophilic properties [22]. In this section, we study the influence of thickness and morphology on the photo-hydrophilic properties of MS and CS films. For all films presented here, occurrence of superhydrophilicity under UV exposure proceeded through a bi-regime mechanism that is illustrated in the inset of Fig. 8. In a first regime, the water contact angle did not vary appreciably over a certain UV exposure duration, which depended on the film thickness or morphology and will be discussed below. In a second regime, the contact angle decreased rapidly under UV exposure, reaching a value of zero within a few minutes. Let us recall that in this study, photo-hydrophilicity is characterized by the photo-wettability duration, i.e. the UV illumination duration

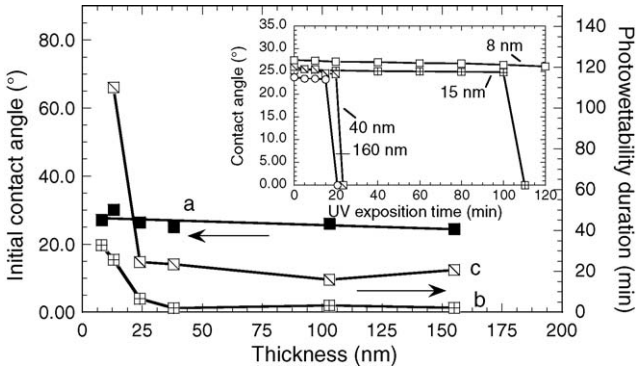

Fig. 8. Influence of thickness on: (a) the natural water contact angle and (b and c) the photo-wettability duration measured for a film–lamp distance of: (b) 5 cm and (c) 30 cm. Measurements were performed on MS films heat-treated at 500 °C. Inset shows the thickness influence on contact angle variations under UV exposition for MS films heat-treated at 500 °C and a film–lamp distance of 30 cm.

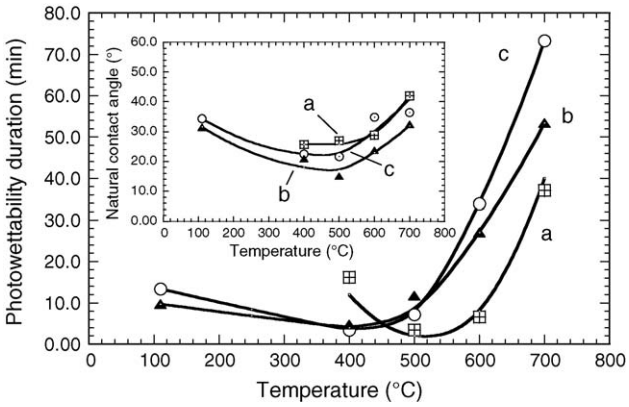

Fig. 9. Photo-wettability duration vs. annealing temperature for: (a) MS, (b) CS/10/200 and (c) CS/90/130 films. Inset shows the natural water contact angle variations for the same films.

necessary for reaching a contact angle of zero, which therefore accounts for the total duration of both regimes.

We first paid attention to the influence of film thickness on the photo-hydrophilic properties. Since the occurrence of superhydrophilicity not only depends on photo-induced properties of the film but can also be influenced by its natural hydrophilicity, the natural contact angle of MS and CS films has first been measured before UV exposure. For both kinds of films, we did not observe any significant influence of the film thickness on the natural hydrophilicity. This is illustrated in Fig. 8a for MS films heat-treated at 500 °C. The contact angle lies in a range 25–30° for any thicknesses. This invariance is primarily related to the fact that morphologic properties discussed in the first section, which might influence the natural wettability, do not appreciably evolve with film thickness. Fig. 8b and c shows that the photo-wettability mechanism follows two kinds of behaviors, depending on whether the thickness is smaller or greater than a threshold value of around 25 nm. For very thin films, i.e. a thickness smaller than the threshold value, the photo-wettability duration noticeably decreases with increasing film thickness. As shown in inset of Fig. 8, the thickness essentially influences the duration of the first photo-wettability regime, where the contact angle does not appreciably vary with UV exposition time. Above the threshold value, the thickness does not promote further photo-wettability variations. This feature indicates that, contrary to the photocatalytic activity that continuously increases with thickness, photo-induced hydrophilicity only involves a very thin active layer at the outer surface of the film. The role of this surface layer will be discussed below. Fig. 8b and c also indicate that, for a fixed thickness, the wettability duration decreases with decreasing the distance between film surface and UV lamp. For instance, when the film–lamp distance was fixed at 5 cm, no first regime could be evidenced for MS films heat-treated at 500 °C with a thickness of 40 nm or more (not illustrated here), while a first regime duration of around 20 min was evidenced for the same films with a film–lamp distance of 30 cm (inset of Fig. 8). These features presumably indicate that a higher UV intensity promotes a more efficient charge carrier generation that increases the photo-wettability rate. In next studies, the film–lamp distance has been fixed at 5 cm and the film thickness at 40 nm, i.e. a thickness greater than the previously depicted threshold value.

Fig. 9 illustrates natural and photo-induced wettability properties of MS, CS/10/200 and CS/90/130 films heat-treated at various temperatures. Inset of Fig. 9 indicates that all films are poorly hydrophilic and, though surface morphologies of the three series strongly vary with the sol nature, this parameter does not influence much the natural hydrophilicity of derived films, which is therefore essentially influenced by intrinsic properties of crystallites at the film surface. Fig. 9 also shows that the natural contact angle is weakly influenced by the heat-treatment temperature. For the three series, the contact angle slightly decreases when increasing the temperature up to 500 °C, reaching a value around 20–30°, and then slightly increases with further temperature increase. These small variations have not been elucidated yet. In contrast to natural wettability, the photo-induced superhydrophilicity strongly depends on the MS or CS sol nature and heat-treatment temperature. It means that the film morphology significantly influences photo-wettability mechanisms. As already depicted in Fig. 8 for the thickness influence, morphology features essentially promoted variations in the duration of the first photo-wettability regime and no important variation could be evidenced concerning the second regime. First of all, it is not excluded that natural wettability influences the photo-induced superhydrophilicity. However, no clear correlation could be established between both properties. For instance, considering films heated at 500 °C, the CS/10/200 film exhibits the best natural hydrophilicity, while the MS film exhibits the worst (inset of Fig. 9). This order is reversed as concerns photo-hydrophilicity (Fig. 9). In contrast, a comparison of Figs. 7 and 9 shows that photocatalytic activity and photo-hydrophilicity follow rather similar trends. On the one hand, for CS/10/200 and CS/90/130 films, best photo-hydrophilic properties are obtained after heat-treatment at 400 °C or less. In this thermal range, the photo-wettability duration undergoes only weak variations with temperature, as also observed for the photocatalytic activity. For further temperature increase up to 700 °C, the photo-

wettability duration is observed to increase by about one order of magnitude, indicating a strong loss of photo-hydrophilicity that correlates the decrease of photocatalytic activity. On the other hand, amorphous MS films do not exhibit any photo-hydrophilic properties. This observation confirms that, like photocatalysis, photo-hydrophilicity requires well-crystallized films that guarantee efficient generation and transfer of charge carriers. For crystalline MS films, best photo-hydrophilic properties are obtained after heat-treatment at 500–600 °C, while heating at 700 °C promotes a significant loss of photo-hydrophilicity, which again correlates photocatalytic activity variations.

Comparable trends illustrated in Figs. 7 and 9 indicate that morphologic features, which are in turn related to the sol nature and heat-treatment temperature, similarly influence photocatalytic and photo-hydrophilic properties. This primarily ensues from the fact that both properties are governed by a same migration mechanism of photo-generated charge carriers toward film surface. This migration competes with charge carrier recombination that is controlled by primary and secondary particle sizes for MS and CS films, respectively. However, some small discrepancies exist between trends illustrated in Figs. 7 and 9. On the one hand, no significant difference can be observed in the photo-hydrophilicity of CS/10/200 and CS/90/130 films heat-treated up to 500 °C, and the photo-hydrophilicity of the former is lower than that of the latter after heat-treatment at higher temperature. In contrast, CS/10/200 films exhibit a greater photocatalytic activity at any temperature. This difference indicates that a possible liquid impregnation within the deeper layers of the more porous CS/10/200 film does not improve photo-hydrophilicity, contrary to what is observed for the photocatalytic activity. On the other hand, optimum photo-hydrophilic properties of CS and MS films, which are measured after heat-treatment at 400 °C or less and at 500–600 °C, respectively, are very comparable. For these films the photo-wettability duration lies between 5 and 10 min, and the duration of the first regime is extremely short or even not measurable. In contrast, photocatalytic activities of the same films are appreciably different, as shown in Fig. 7a and c. It is inferred that, owing to a much shorter migration pathway across the thin active surface layer, which implies a much lower recombination probability of charge carriers, photo-hydrophilic properties are less sensitive to morphology variations that influence surface and volume recombination mechanisms. Despite these small differences, common trends illustrated in Figs. 7 and 9 clearly show that photocatalytic and photo-hydrophilic properties, which complementary act for self-cleaning applications, can be simultaneously optimized after heat-treatment at a given temperature that depends on the sol formulation, i.e. at 400 °C or less or at 500–600 °C for films deposited from CS or MS sols, respectively. We believe that these common trends can also be discussed in terms of mutual influence of photocatalytic and photo-hydrophilic mechanisms. First of all, photo-hydrophilicity can participate to the photocatalytic process. It is known that, in aqueous media, the photocatalytic reaction proceeds through oxidative decomposition mechanisms, where strongly oxidant $OH^{\bullet}$ radicals are the essential reactant [21]. These radicals originate from the oxidation by photo-generated holes of OH^{-} groups present at the titania surface. We have previously indicated that photo-hydrophilicity occurs through a photo-induced molecular or dissociative water adsorption at the film surface, thus promoting an enhanced amount of OH^{-} groups at the surface. These groups can then be oxidized by photo-holes. It is therefore likely that photo-hydrophilicity enhances the photocatalytic activity in aqueous medium by promoting the formation of $OH^{\bullet}$ oxidative radicals at the film surface.

Photocatalytic mechanisms can in turn favorably act on the photo-hydrophilicity by promoting carbon decontamination at the film surface. We have shown in another article that carbon contamination naturally occurs during film aging in room atmosphere, which rapidly impinges the hydrophilic properties of TiO_2 films [27]. It is the reason why in the present work, in order to minimize aging effects and for a comparative purpose, hydrophilic properties were systematically investigated within the first 24 h following film deposition. However, this unavoidable contamination can be eliminated through photocatalytic mechanisms. This feature has been investigated on four identical MS films heat-treated at 500 °C, which were preliminary aged for 1 week in room atmosphere before study in order to enhance contamination. Photo-induced variations of the water contact angle were measured with respect to UV exposure time and the four films were subsequently studied by XPS with respect to the C 1s peak (284.7 eV), after an UV exposure of 0, 10, 20, and 150 min, respectively. FTIR and XPS studies did not allow detecting any remaining alkoxy groups arising from the titanium alkoxide precursor (not illustrated here), which might contribute to the C 1s peak. It is thus concluded that the C 1s peak essentially reflects carbon contamination at the film surfaces. The film hydrophilicity was not further investigated after XPS analysis because the ultra high vacuum used for XPS studies could promote changes in the surface properties. In particular, it is worthwhile mentioning that XPS data reported hereafter are not directly representative of the actual carbon contamination, since the ultra high vacuum can promote partial carbon desorption. Thus, XPS data are only studied from a comparative point of view. Fig. 10 shows variations of the C 1s peak with UV exposure time. A clear correlation exists with water contact angle variations that are illustrated in the inset of Fig. 10. The initial contact angle of 52° is much greater than that depicted in Figs. 8 and 9 for fresh films owing to a greater carbon contamination related to preliminary aging. The contact angle varies very weakly over the first 20 min of UV exposure, which traduces occurrence of the first photo-wettability regime. In the same time, Fig. 10 shows that the C 1s peak intensity readily decreases. For a longer UV exposure, this peak no longer decreases in intensity, while Fig. 10 shows a marked decrease of the contact angle that illustrates occurrence of the second photo-wettability regime. These data suggest following interpretation for both regimes. The first one would be dominated by the partial photocatalytic decomposition of carbon contamination promoted by photo-generated charge carriers. It is not excluded that oxygen vacancies can also be formed during this first regime through an interaction of surface oxygen with

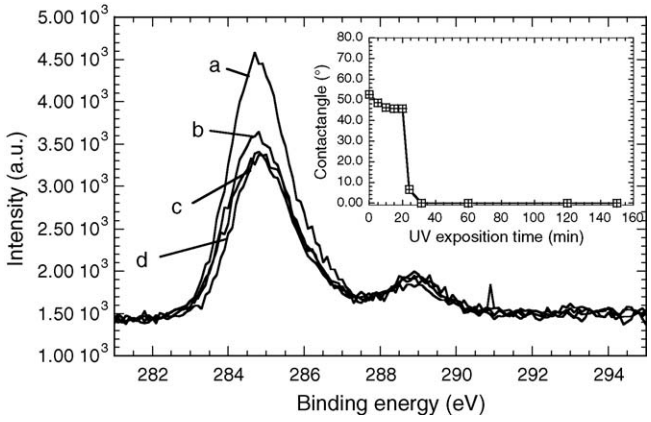

Fig. 10. C 1s peak measured by XPS for MS films heat-treated at 500 °C, aged in room atmosphere for 1 week, and exposed to UV radiation for: (a) 0 min, (b) 10 min, (c) 20 min, and (d) 150 min. Inset shows corresponding water contact angle variations.

photo-holes. However, no important wettability modification is observed, which traduces that carbon contamination screens the surface and impinges water adsorption by oxygen vacancies. After a sufficient exposure time, i.e. below a certain decontamination threshold, which essentially depends on morphologic characteristics of the films, the photocatalytic process ceases, and the water contact angle rapidly decreases yielding superhydrophilicity. These observations suggest that, during the second wettability regime, (i) all photo-generated holes are now consumed by surface oxygen to form vacancies and (ii) the surface is sufficiently decontaminated for allowing oxygen vacancies to adsorb water. According to this, it can then be concluded that the active surface layer depicted in Fig. 8, which governs photo-hydrophilic features and principally the duration of the first regime, corresponds to the amount of TiO_2 required for promoting a sufficient flux of charge carrier necessary to promote: (i) a partial photocatalytic decontamination of the film surface and (ii) a saturation of the decontaminated surface with oxygen vacancies.

4. Conclusion

TiO_2 films were deposited using various sol–gel routes. This study shows that the morphology of TiO_2 films closely depends on the experimental conditions. The crystallite size and densification degree are strongly influenced by the sol nature and post-deposition heat-treatment temperature, and range between 6 and 60 nm and between 12 and 50 vol%, respectively. The existence and size of secondary aggregated particles is also determined by the sol nature. Primary single-crystal particles and secondary aggregated polycrystalline particles act in turn on the pore size and surface roughness. Thus, a suitable control of the experimental conditions allowed covering a large variety of morphologies. The photo-induced properties of TiO_2 films were then studied with respect to their morphologies. Photo-induced properties of sol–gel films in aqueous medium are essentially controlled by a migration of photo-generated charge carriers from deeper layers toward surface of the film. This migration is affected by multiple recombination mechanisms at the surface or within the volume of primary or secondary particles constituting the films. An efficient charge carrier transfer through the thickness requires optimum particle size and film densification in order to minimize the recombination probability. The photo-induced superhydrophilicity depends less critically on the film morphology than the photocatalytic activity. It is because only a thin active surface layer is involved in the former, which reduces the recombination probability during migration of charge carriers toward surface, while the whole film thickness is involved in the latter. However, this study shows that both properties follow similar general trends with respect to morphology, which not only ensues from the fact that they are governed by same mechanisms but also suggests their mutual influence. Consequently, both properties that complementary act for self-cleaning applications can be simultaneously optimized. According to different influences of the film morphology, best photo-induced properties are obtained after a heat-treatment at 400 °C or less or at 500–600 °C for films deposited from crystalline suspensions or polymeric sols, respectively.

References

[1] A. Fujishima, K. Honda, Nature 238 (1972) 37.
[2] O. Carp, C.L. Huisman, A. Reller, Prog. Solid State Chem. 32 (2004) 33.
[3] J.M. Herrmann, H. Tahiri, C. Guillard, P. Pichat, Catal. Today 54 (1999) 131.
[4] Z. Zhang, C.C. Wang, R. Zakaria, J.Y. Ying, J. Phys. Chem. B 102 (1998) 10871.
[5] A.J. Maira, K.L. Yeung, C.Y. Lee, P.L. Yue, C.K. Chan, J. Catal. 192 (2000) 185.
[6] S. Ito, S. Inoue, H. Kawada, M. Hara, M. Iwasaki, H. Tada, J. Colloid Interface Sci. 216 (1999) 59.
[7] J.F. Porter, Y.G. Li, K.C.K. Chan, J. Mater. Sci. 34 (1999) 1523.
[8] C.H. Cho, D.K. Kim, J. Am. Ceram. Soc. 86 (7) (2003) 1138.
[9] A. Fernandez, G. Lassaletta, V.M. Jimenez, A. Justo, A.R. Gonzalez-Elipe, J.M. Herrmann, H. Tahiri, Y. Ait-Ichou, Appl. Catal. B: Environ. 7 (1995) 49.
[10] J.C. Yu, W. Ho, J. Lin, H. Yip, P.K. Wong, Environ. Sci. Technol. 37 (2003) 2296.
[11] V. Roméas, P. Pichat, C. Guillard, T. Chopin, C. Lehaut, Ind. Eng. Chem. Res. 38 (1999) 3878.
[12] R. Wang, N. Sakai, A. Fujishima, T. Watanabe, K. Hashimoto, J. Phys. Chem. B 103 (1999) 2188.
[13] T. Watanabe, A. Nakajima, R. Wang, M. Minabe, S. Koizumi, A. Fujishima, K. Hashimoto, Thin Solid Films 351 (1999) 260.
[14] Y. Paz, Z. Luo, L. Rabenberg, A. Heller, J. Mater. Res. 10 (11) (1995) 2842.
[15] A. Mills, A. Lepre, N. Elliott, S. Bhopal, I.P. Parkin, S.A. O'Neill, J. Photochem. Photobiol. A: Chem. 160 (2003) 213.
[16] A. Mills, G. Hill, M. Crow, S. Hodgen, J. Appl. Electrochem. 35 (2005) 641.
[17] M. Langlet, A. Kim, M. Audier, C. Guillard, J.M. Herrmann, J. Mater. Sci. 38 (2003) 3945.
[18] M. Fallet, S. Permpoon, J.L. Deschanvres, M. Langlet, J. Mater. Sci., in press.
[19] M. Born, E. Wolf, Principle of Optics, Pergamon, New York, 1975, p. 85.
[20] R.C. Weast (Ed.), Handbook of Chemistry and Physics, 48th ed., The Chemical Rubber Co., Cleveland, OH, 1967, p. B-279.
[21] J.M. Herrmann, Catal. Today 53 (1999) 115.

[22] S. Permpoon, M. Fallet, G. Berthome, B. Baroux, J.C. Joud, M. Langlet, J. Sol–Gel Sci. Tech. 35 (2005) 127.
[23] G. Baldinozzi, D. Simeone, D. Gosset, M. Dutheil, Phys. Rev. Lett. 90 (21) (2003) 216103.
[24] G.J. Exarhos, N.J. Hess, Mater. Res. Soc. Symp. Proc. 271 (1992) 319.
[25] C.J. Brinker, G.W. Scherer, Sol–Gel Science, The Physics and Chemistry of Sol–Gel Processing, Academic Press, San Diego, 1990, pp. 675–742.
[26] K. Terabe, K. Kato, H. Miyazaki, S. Yamaguchi, A. Imai, Y. Iguchi, J. Mater. Sci. 29 (1994) 1617.
[27] S. Permpoon, G. Berthomé, B. Baroux, J.C. Joud, M. Langlet, J. Mater. Sci., in press.